American Mineralogist, Volume 92, pages 1054–1063, 2007

Crystal chemical relationships in the tourmaline group: Structural constraints on chemical variability

FERDINANDO BOSI[1,*] AND SERGIO LUCCHESI[2]

[1]Department of Mineralogy, Swedish Museum of Natural History, Box 50007, 10405 Stockholm, Sweden
[2]Dipartimento di Scienze della Terra, Università degli Studi di Roma "La Sapienza," P.le A. Moro 5, 00185 Roma, Italy

ABSTRACT

This paper explores some aspects of the crystal chemistry and structural constraints on tourmaline by examining 127 samples from the literature. According to the bond-valence model, the tourmaline structure shows lattice-induced strain at each polyhedron. The overall effect is an expansion of the triangular (BO_3) group and compression of the tetrahedron. The X polyhedron can be either compressed or expanded: compression increases with vacancy content, whereas expansion is typical of Ca-rich tourmaline. The Y octahedron changes extensively from compressed through an unstrained to expanded state as a function of increasing Li content. The Z octahedron is almost unstrained in crystals with $\Sigma^{Z}R^{2+} < 0.40$ apfu, whereas it is compressed in crystals with $\Sigma^{Z}R^{2+} > 0.40$ apfu.

The configuration of the six-membered tetrahedral ring is strongly affected by <Y-O>, which is the most important parameter linked to the deviation of the tetrahedral ring from hexagonal symmetry. The whole structure is stable when the channels through the Z octahedron framework are able to accommodate the Y cations. As <Y-O> becomes larger, the less puckered the tetrahedral ring and the more the O7 atom is displaced away from Z. Consequently, the difference between <Y-O> and <Z-O> cannot be too large, otherwise <Z-O> will be too small to be commensurate with shifting of the O7 atom. One possible mechanism to reduce the difference between <Y-O> and <Z-O>, is the disordering reaction $^{Y}Al + {}^{Z}R \rightarrow {}^{Y}R + {}^{Z}Al$, which increases <Z-O> and decreases <Y-O>. In ideal dravite, schorl, and "tsilaisite," <Y-O> and <Z-O> are incommensurate.

Keywords: Order-disorder, crystal structure, tourmalina, XRD data

INTRODUCTION

The general formula of tourmaline may be written as $XY_3Z_6(T_6O_{18})(BO_3)_3V_3W$, where: X = □, Na, K, Ag, Ca; Y = Li, Mg, Fe^{2+}, Mn^{2+}, Zn, Al, Fe^{3+}, Cr^{3+}, V^{3+}, Ti^{4+}, □; Z = Mg, Fe^{2+}, Al, Fe^{3+}, Cr^{3+}, V^{3+}; T = Si, Al, B, Be; B = B, (□); V = OH, O; W = OH, F, O (according to chemical formulae of Hawthorne and Henry 1999; Bosi and Lucchesi 2004; Hughes et al. 2004; London et al. 2006). The complexity of the tourmaline structure allows great compositional flexibility, often associated with non-convergent ordering at the Y and Z sites (e.g., $^{Y}Mg + {}^{Z}Al \rightarrow {}^{Y}Al + {}^{Z}Mg$, Hawthorne et al. 1993). The structure is characterized by ditrigonal rings of six tetrahedra (T_6O_{18}). Triangular groups (BO_3) oriented sub-parallel to (0001) lie between the tetrahedral rings. The tetrahedra are bonded, through their apices, to two types of octahedra, Y and Z, and share one edge (O4-O5) with the trigonal antiprism X. Three Y octahedra each share two edges (O1-O2) and surround the threefold axes. The groups of (XO_9), (YO_6), (TO_4) polyhedra, and B-centered polyhedra connect to each other through (ZO_6) octahedra, which form a three-dimensional framework. The Z octahedra share two equivalent edges, O7E-O8 and O7D-O8E (according to the symbols used by Foit 1989), and link to the Y octahedron through the O3-O6 edge.

This paper explores the crystal structures of tourmaline with different chemical compositions using the bond-valence model. It develops an empirical crystal-chemical model, which shows the geometrical constraints needed for the stability of this mineral.

SAMPLES

Data for 127 crystal-structural refinements of tourmaline were taken from the literature (Table 1). However, some reported bond distances were erroneous. In the OlnG sample (Gorskaya et al. 1982) the bond distances were recalculated from positional parameters, showing that the Z-O8E bond distance is not 1.826 but 1.886 Å: consequently, the <Z-O> mean bond distance changes from 1.898 to 1.908 Å. A similar situation was observed for samples LidA1 and LidA2 (Aurisicchio et al. 1999). The O1 positional parameter was refined and found to be displaced from the threefold axis to the mirror plane. This yielded three Y-O1 bond distances split into two long and one short, and not three long distances, as reported by the above authors. The actual Y-O1 bond distances are 2.183(×2) and 1.784 Å for LidA1, and 2.178(×2) Å and 1.782 Å for LidA2. Consequently, the respective overall <Y-O> mean bond distances change from 2.066 to 2.043 Å, and from 2.063 to 2.041 Å for LidA1 and LidA2, respectively.

Samples PovGE and FuvGE (Grice and Ercit 1993) and BrgG (Barton 1969) are the same as those Grice et al.'s (1993) povondraite, Grice and Robinson's (1989) feruvite, and Tippe

* E-mail: ferdinando.bosi@uniroma1.it

and Hamilton's (1971) buergerite, respectively. Therefore, only the first three samples were used. The elbaite of Donnay and Barton (1972) is the same as that of Donnay (1977). The latter was preferred, because the chemical composition more closely fits the structural parameters. Nuber and Schmetzer (1979) only report cation distribution in the octahedral sites of chromdravite, so that only Y and Z content and the structural parameters were used. The olenite samples of Marler et al. (2002) show experimental errors related to bond distances that were too large for the present purposes and were consequently discarded.

Formula optimization

In the last few years, good approaches toward optimizing site assignments in tourmaline have been developed (Wright et al. 2000; Bosi and Lucchesi 2004; Bosi et al. 2005a, 2005b). These methods combine structural and chemical data by means of a quadratic program solver to minimize residuals between observed and calculated parameters. The mathematical robustness of these procedures allows us to re-examine previously published crystal-chemical formulae, whose atom distribution at the T, Y, and Z sites were not obtained in this manner. The first optimization cycle was carried out using the procedure of Wright et al. (2000), and the last using the procedure of Bosi et al. (2005a, 2005b) with the ionic radii of Table 2. Both methods provide comparable results. The corresponding T, Y, and Z site populations are listed in Table 3.

The ionic radii (Table 2) fit 93% of T, Y, and Z mean bond distances within experimental error (2 estimated standard deviations) in all samples used in the current study. Their success is shown by the residuals between the observed and the calculated mean bond distances (Fig. 1).

The ionic radii of Al and Fe^{3+}

The ionic radii of Al and Fe^{3+} vary at the same site because of the following factors: (1) the high ionic potential (ip = z/r, where z = atomic valence, r = ionic radius) of Al^{3+} produces intense cation-cation repulsion among adjacent octahedra; (2) the tendency of Y to compress Z; (3) order-disorder partitioning

Table 1. List of examined samples

Cempírek et al. (2006)	Fe-OlnC
London et al. (2006)	Ag-TM
Bosi et al. (2005b)	66c, 61Rda, 60fc, 62ha, 64gh, L4e, 61Vbh, L4c, L3h, L4b, L4d, L1v, L1z
Bosi et al. (2005a)	Elb2rim, Tsl2y, Tsl2z, Tsl2w, Tsl2x, Tsl2m, Tsl2g
Ertl et al. (2005)	REDT1, REDT2
Marschall et al. (2004)	SY309B
Ertl et al. (2004b)	Fe-OlnE*
Ertl et al. (2004a)	T2Mn
Hughes et al. (2004)	T1, T2, T3. T4, T5
Bosi et al. (2004)	TMt3b, Tmt6b, TMt3c, TMpr79f, TM1p43e
Bosi and Lucchesi (2004)	TM507c, TM507e, TM504c, TM9840c, TM9840f, TM9914b, TM235a, TM235b, TM65e, TM60e, TM233g, TM501e, TM84a, TM112a, TM112c, TMl2ap, TMl2al, TMl3l, TMl4aa
Ertl et al. (2003b)	GOS1, GOS2
Ertl et al. (2003a)	BT, P6
Cámara et al. (2002)	Elb19*, Sch16*, Drv18*
Schreyer et al. (2002)	OlnS
Ertl et al. (2002)	Elb-Cu
Ertl and Hughes (2002)	SchE
Hughes et al. (2000)	OlnH
Kahlenberg and Veličkov (2000)	FoitKV
Francis et al. (1999)	FoitF
Bloodaxe et al. (1999)	108749, Dlux1, HP21, LCW2356, OT1692, No32008, SmFalls, RuT1792, RuT1892
Aurisicchio et al. (1999)	LidA1, LidA2
Selway et al. (1998)	Ross
Taylor et al. (1995)	UviT*
MacDonald and Hawthorne (1995b)	T72*, T73*, T74*, T75*, T76*,T77*, T78*, T79*, T80*
MacDonald and Hawthorne (1995a)	T54, T55
Burns et al. (1994)	NP1, NP2, NP3, T10, T11, T12, T15, SD
MacDonald et al. (1993)	FoitM*
Hawthorne et al. (1993)	DrvH*
Grice and Ercit (1993)	BrgGE*, FuvGE*, PovGE*, ElbGE*, S2672*, S49356*, Scross*, D32008*, D43167*, D43873*, D43230*, UviGE*
Foit (1989)	SchF*
Nuber and Schmetzer (1984)	TslN
Gorskaya et al. (1982)	OlnG
Nuber and Schmetzer (1981)	LidNS
Nuber and Schmetzer (1979)	CrDrvNS*
Foit and Rosenberg (1979)	VDrv*
Schmetzer et al. (1979)	DrvNSA*, UviSNA*
Donnay (1977)	ElbD
Fortier and Donnay (1975)	SchFD*
Barton (1969)	BrgB*
Buerger et al. (1962)	UviB* (Chemism by Donnay and Barton 1972)

* Formula optimized by Wright et al. (2000) and Bosi et al. (2005a, 2005b) procedures.

[1] Deposit item AM-07-028, Table 3 (T, Y, and Z site populations). Deposit items are available two ways: For a paper copy contact the Business Office of the Mineralogical Society of America (see inside front cover of recent issue) for price information. For an electronic copy visit the MSA web site at http://www.minsocam.org, go to the American Mineralogist Contents, find the table of contents for the specific volume/issue wanted, and then click on the deposit link there.

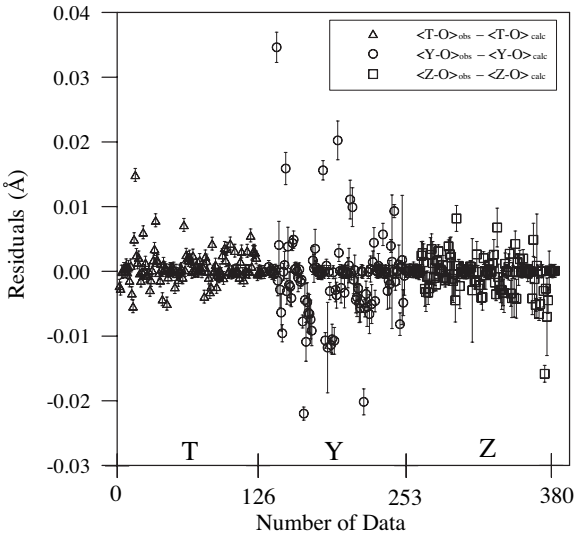

Figure 1. Plot of the residuals between observed and calculated <T-O>, <Y-O>, and <Z-O> mean bond distances. The vertical bars represent the average estimated standard deviation (±1σ) quoted by the authors. Note that 96, 86, and 96% of <T-O>, <Y-O>, and <Z-O> evaluations, respectively, are within ±2σ.

Table 2. Ionic radii in tourmaline (Å)

	Y site	Z site	T site
Si^{4+}			0.259
Ti^{4+}	(0.605)		
B^{3+}			(0.11)
Al^{3+}	0.547	0.550, for $^{Z}\Sigma R^{2+} < 0.40$ apfu; 0.543, for $^{Z}\Sigma R^{2+} > 0.40$	(0.39)
Fe^{3+}	0.697; (0.645), for $^{Y}Fe^{3+} > {}^{Y}Al$	0.705, for $^{Z}\Sigma R^{2+} < 0.40$; 0.698, for $^{Z}\Sigma R^{2+} > 0.40$; (0.645), for $^{Z}Fe^{3+} > {}^{Z}Al$	
Cr^{3+}	0.617	0.613	
V^{3+}	0.657	0.653	
Fe^{2+}	0.778	0.774	
Mn^{2+}	0.809	0.809	
Mg^{2+}	0.723	0.720	
Zn^{2+}	(0.74)		
Cu^{2+}	(0.73)		
Be^{2+}			(0.27)
Li^{+}	0.751		
Vacancy	2.11; 2.25, for olenite		

Notes: Uncertainty estimated at ca. 0.001 Å; the vacancy size (estimated in this work) is defined as "bond distance." Ionic radii obtained from Bosi et al. (2005a, 2005b, 2004). Parentheses = ionic radii from Shannon (1976). The mean Y and Z anionic radii are functions of constituent-anion radius of Shannon (1976). The $<^{Y}$a.r.> change from 1.353 to 1.363 Å. The $<^{Z}$a.r.> = 1.357 Å for nearly all samples, except the samples with oxygen at the V-site, such as the buergerites.

of cations at octahedral sites; and (4) the Fe^{3+} cation is "softer" and more electronegative than Al.

Normally, if the ionic potential increases in a polyhedron, the edge shared with another polyhedron contracts, to more effectively screen the cation. As a result, the cation is displaced from its polyhedral center, away from the shared edge (Pauling's rules), and the mean bond distance may change according to the distortion theorem (Brown 2002). In tourmaline, the Z cation shift (Z-O7D + Z-O7E)/(Z-O3 + Z-O6) is the parameter that reflects how the Z cation moves away from the O3-O6 shared edge toward the O7D-O7E edge (Foit 1989). The Z cation shift shows a negative correlation with the mean ionic potential ratio $<ip_Y>/<ip_Z>$ (Fig. 2); i.e., the Z octahedron tends to be compressed by Y. However, this compression is only effective (i.e., Z polyhedron size decreases) if $^{Z}R^{3+}$ has a $^{Z}R^{2+}$ cation as its second neighbor, and not another $^{Z}R^{3+}$ cation. In fact, $^{Z}R^{3+}$-$^{Z}R^{3+}$ cation repulsion prevents Z compression, because the repulsion in Z is so intense that the <Z-O> mean bond distance cannot change. This phenomenon is illustrated by the <Z-O> vs.O7E-O8 shared edge plot (Fig. 3). In samples with the sum of divalent cations at the Z site ($\Sigma^{Z}R^{2+}$) < 0.40 atoms per formula unit (apfu), there is intense Al^{3+}-Al^{3+} repulsion among the Z octahedra and, although O7E-O8 increases, <Z-O> remains almost constant. In contrast, in samples with $\Sigma^{Z}R^{2+} > 0.40$ apfu, Z-Z repulsive forces decrease and, in turn, <Z-O> and O7E-O8 increase together, according to the following function:

$$<\text{Z-O}> = 0.648 \cdot (\text{O7E-O8}) + 0.360 \ (r^2 = 0.96)$$

It should be noted that extrapolation of this function to small O7E-O8 values (typical of $^{Z}Al \cong 6$ apfu) leads to <Z-O> values smaller than those ever observed. In addition, $^{Y}R^{2+} + {}^{Z}R^{3+} \rightarrow {}^{Y}R^{3+} + {}^{Z}R^{2+}$ order-disorder reactions support enhancement of the mean ionic potential ratio of Y to Z, allowing decrease of the $^{Z}Fe^{3+}$ and ^{Z}Al ionic radius by 0.007 Å (Table 2).

Fe^{3+} is soft enough to decrease its size by an additional 0.053 Å (e.g., PovGE, D43167, D43873, Drv18). Consequently, Fe^{3+} will have shorter and stronger bonds, and an increased covalent character according to the bond valency theory (Brown and Shannon 1973; Brown 2002). This phenomenon is effective at the Y site for $^{Y}Fe^{3+} > {}^{Y}Al$ and at the Z site for $^{Z}Fe^{3+} > {}^{Z}Al$. In fact, the cation-cation repulsive forces regarding Fe^{3+} are not as intense as for the $Fe^{3+} < Al$ case because the covalent character of Fe^{3+} increases the shielding effect of the anions forming polyhedral-shared edges (Tossel and Gibbs 1977; Hill et al. 1983; Nakatsuka et al. 1995, 1999).

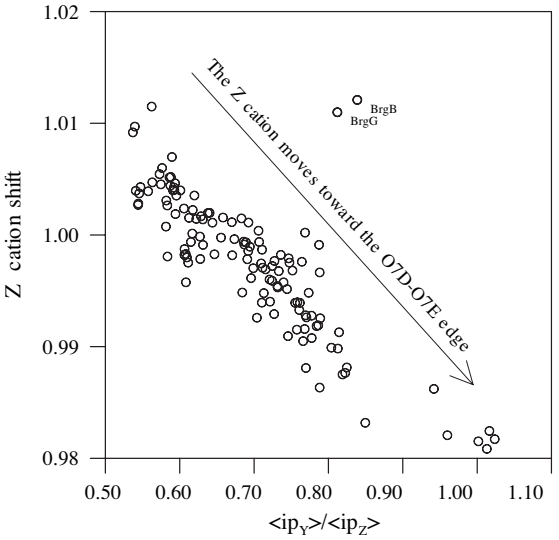

Figure 2. With an increase in density of charge at the Y site, the Z cation moves toward the O7D-O7E edge. As a result, the Z-octahedra may become compressed.

Bond-valence approach

The properties of the tourmaline structure can be studied by bond-valence theory. The bond valence S_{ij} of a bond between ions i and j is given by $S_{ij} = \exp[(R_0 - R_{ij})/0.37]$, where R_0 is an empirical parameter whose values for different bonds have been tabulated by Brown and Altermatt (1985) and Brese and O'Keeffe (1991), and R_{ij} is the bond distance between ion i and neighboring ion j. In all samples, experimental bond valences S_{ij} were calculated from the observed bond distances, and ideal (theoretical) bond valences s_{ij} (Brown 2002) by the bond graph

TABLE 4. Solution of network equations related to tourmaline bond graph

$sYO1 = (1/3 \cdot O1)$
$sXO2 = 1/1297 \cdot [-5220 - (166/3 \cdot O1) - (242 \cdot O3) + (805/3 \cdot X) + (872 \cdot T) + (166 \cdot Y) + (560 \cdot Z)]$
$sYO2 = 1/1297 \cdot [-4186 - (953/6 \cdot O1) - (733/2 \cdot O3) + (166/3 \cdot X) + (581 \cdot T) + (953/2 \cdot Y) + (623 \cdot Z)]$
$sBO2 = 1/1297 \cdot [-3269 - (178/3 \cdot O1) - (322 \cdot O3) + (160/3 \cdot X) + (560 \cdot T) + (178 \cdot Y) + (788 \cdot Z)]$
$sYO3 = 1/1297 \cdot [2104 - (110/3 \cdot O1) + (1691/3 \cdot O3) - (76/3 \cdot X) - (266 \cdot T) + (110 \cdot Y) - (504 \cdot Z)]$
$sZO3 = 1/1297 \cdot [-1052 + (55/3 \cdot O1) + (1100/3 \cdot O3) + (38/3 \cdot X) + (133 \cdot T) - (55 \cdot Y) + (252 \cdot Z)]$
$sXO4 = 1/1297 \cdot [2610 + (83/3 \cdot O1) + (121 \cdot O3) + (82 \cdot X) - (436 \cdot T) - (83 \cdot Y) - (280 \cdot Z)]$
$sTO4 = 1/1297 \cdot [-8 - (83/6 \cdot O1) - (121/2 \cdot O3) - (41 \cdot X) + (218 \cdot T) + (83/2 \cdot Y) + (140 \cdot Z)]$
$sYO6 = 1/1297 \cdot [3134 - (39 \cdot O1) + (254/3 \cdot O3) - (128/3 \cdot X) - (448 \cdot T) + (117 \cdot Y) - (371 \cdot Z)]$
$sZO6 = 1/1297 \cdot [-22 + (16 \cdot O1) - (337/3 \cdot O3) - (14/3 \cdot X) - (49 \cdot T) - (48 \cdot Y) + (385 \cdot Z)]$
$sTO6 = 1/1297 \cdot [-518 + (23 \cdot O1) + (83/3 \cdot O3) + (142/3 \cdot X) + (497 \cdot T) - (69 \cdot Y) - (14 \cdot Z)]$
$sZO7D = 1/1297 \cdot [1030 - (7/3 \cdot O1) - (140/3 \cdot O3) - (52/3 \cdot X) - (182 \cdot T) + (7 \cdot Y) + (133 \cdot Z)]$
$sTO7 = 1/1297 \cdot [534 + (14/3 \cdot O1) + (280/3 \cdot O3) + (104/3 \cdot X) + (364 \cdot T) - (14 \cdot Y) - (266 \cdot Z)]$
$sZO8 = 1/1297 \cdot [-493 - (89/6 \cdot O1) - (161/2 \cdot O3) + (40/3 \cdot X) + (140 \cdot T) + (89/2 \cdot Y) + (197 \cdot Z)]$
$sBO8 = 1/1297 \cdot [3580 + (89/3 \cdot O1) + (161 \cdot O3) - (80/3 \cdot X) - (280 \cdot T) - (89 \cdot Y) - (394 \cdot Z)]$

Notes: *s*YO1, *s*XO2, *s*YO2, *s*BO2, *s*YO3, *s*ZO3, *s*XO4 (= *s*XO5), *s*TO4 (= *s*TO5), *s*YO6, *s*ZO6, *s*TO6, *s*ZO7D (= *s*ZO7E), *s*TO7, *s*ZO8 (= *s*ZO8E), *s*BO8 = Ideal bond valence. O1, O3, X, T, Y, Z = mean atomic valence around the respective sites. These equations are valid in the following conditions: O2 = O4 = O5 = O6 = O7 = O8 = 2 v.u., B = 3 v.u.

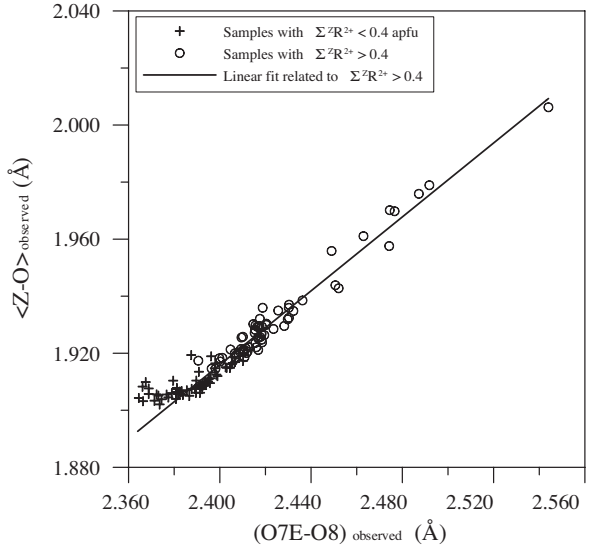

FIGURE 3. Change in <Z-O> vs.O7E-O8 associated with ΣR^{2+} at the Z site.

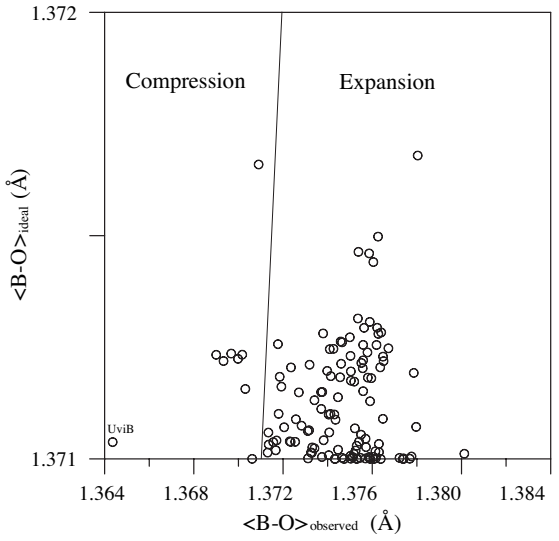

FIGURE 4. $<B\text{-}O>_{ideal}$ vs. $<B\text{-}O>_{obs}$ plot showing the strain state in the triangular $(BO)_3$ groups of tourmalines studied. Solid line: ratio 1:1 between $<B\text{-}O>_{ideal}$ and $<B\text{-}O>_{obs}$ outlining unstrained state.

and network equations related to the tourmaline topology (Table 4). Using s_{ij}, the ideal bond distances for an unstrained tourmaline structure were calculated by the formula: $R_{ij} = R_0 - 0.37 \ln(s_{ij})$. Bond valence results show that the tourmaline structure has lattice-induced strain (Brown 2002). Although the bond strain index values are less than 0.05 valence unit (v.u.), nearly all samples have a global instability indices (GII) > 0.05 v.u. The GII values are indicative of strained bonds, which may lead to an overall effect of compression or expansion in the polyhedra with respect to the unstrained structure. The bond-strain effect reflects departure from 1:1 relation in the ideal and observed mean bond-distance plots for each polyhedron.

Crystal chemistry

B site. All samples have a B content of 3 apfu, within experimental uncertainty. There is no clear experimental evidence of either substoichiometry or of the presence of cations other than boron at the B site. The arithmetic average of all bond distances in B site is 1.374(2) Å. Most samples have observed <B-O> larger than ideal values, so that the overall effect in the triangular (BO_3) group is expansion (Fig. 4).

T site. Silicon is the major cation in the T site. In addition, optimized cation distributions show that Al and B, and occasionally small amounts of Be occur (Hughes et al. 2004). The tetrahedron is quite regular; its distortion $<\lambda_T>$, expressed as quadratic elongation (Robinson et al. 1971), changes from 1.0007 to 1.0050, depending on the charge at X site. Both bond valence sum and mean atomic valence at the X site ($<z_X>$) are positively correlated with $<\lambda_T>$ according to the relationship:

$$<\lambda_T> = 1.0005 + 0.0010 \cdot <z_X> + 0.0008 \cdot <z_X>^2 \ (r^2 = 0.91).$$

The data in Figure 5 shows that the tetrahedra are compressed in nearly all samples. Crimping, ditrigonality, and tetrahedral rotation are the parameters that characterize the configuration of the six-membered tetrahedral ring (Foit 1989). The crimping depends on <Y-O> (Fig. 6a), while the ditrigonality is positively correlated to Mg_{total} (Fig. 6b) and negatively correlated to <Y-O> in the samples with low Mg content ($r^2 = 0.75$). The crimping and the ditrigonality are also influenced by X-O5 (Foit

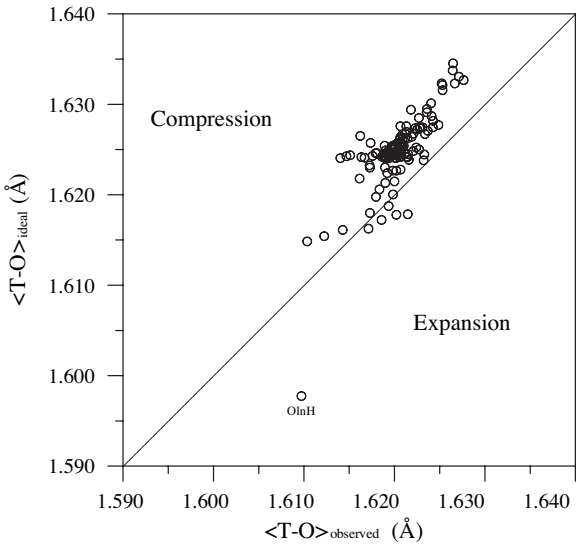

FIGURE 5. <T-O>$_{ideal}$ vs. <T-O>$_{obs}$ plot showing the strain state in the (TO_4) tetrahedra of tourmalines studied. Solid diagonal line: ratio 1:1 between <T-O>$_{ideal}$ and <T-O>$_{obs}$ outlining unstrained state.

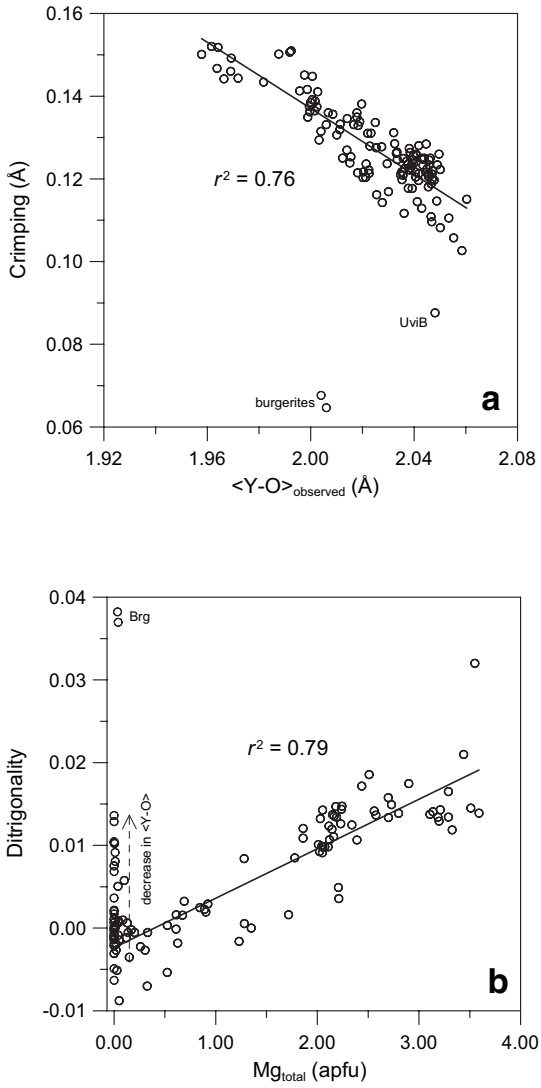

FIGURE 6. Variation of the distortion of the (T_6O_{18}) ring. (**a**) Crimping vs. <Y-O>, the regression line does not include the UviB and buergerite samples. (**b**) Ditrigonality vs. Mg_{total}, the regression line is related to samples with Mg > 0.02 apfu and without buergerite samples.

1989); which may explain why the buergerite samples are off the regression lines (Fig. 6). In fact, small X-O5 bond distances (as in the buergerite) may lead to decrease in the crimping and increase in the ditrigonality (Foit 1989). The tetrahedral rotation shows a negative correlation with <Y-O> (Fig. 7) according to the following relation:

$$\text{Tetrahedral rotation} = 40.312 - 19.651 \text{ <Y-O>} \quad (r^2 = 0.88) \quad (1)$$

With decreasing <Y-O>, the tetrahedra rotate around the O4-O5 edge and the O6 atom is displaced toward the threefold axis, producing puckering of the tetrahedral ring. As a result, the deviation of the tetrahedral ring from hexagonal symmetry is mainly linked to <Y-O>.

X site. Ca, Na, and vacancies occur at the X site. Significant concentrations of K and Ag, more than 0.5 apfu, may also occur (Grice et al. 1993; London et al. 2006, respectively). <X-O> decreases with Ca content and increases with Na content and vacancies (Foit 1989). The X polyhedron can be either compressed or expanded. The strain (calculated as <X-O>$_{ideal}$ – <X-O>$_{obs}$) shows a correlation with the mean atomic valence at the X site (Fig. 8). For $\langle z_X \rangle$ less than ca. 1 v.u. the compression increases considerably, whereas for $\langle z_X \rangle$ more than ca. 1 v.u. the expansion increases slightly. The X strain seems to be linked to the X-atomic valence rather than to the X-cationic size. This might explain the presence of large cation such as K at the X site. Na-occupancy seems to relax the bonds in the X polyhedron, whereas vacancy and Ca induces strain. Compression and expansion are typical of vacancy- and Ca-rich tourmaline, respectively.

Y site. In tourmaline, the Y polyhedron is chemically much more flexible than other polyhedra, being able to incorporate cations of different sizes and charges. Although in all samples <Y-O> decreases with ^{Y}Al content, it also reflects changes due to atom substitutions associated with Al; e.g., the ^{Y}Mg + ^{Z}Al → ^{Y}Al + ^{Z}Mg order-disorder reaction that may occur when ^{Y}Mg → $^{Y}Fe^{2+}$ along the dravite–schorl join. Consequently, <Y-O> does not follow a regular variation with its site population (Fig. 9). Bosi and Lucchesi (2004) called this phenomenon the "cooperative effect."

In nearly all samples, the Y polyhedron edges positively correlate with <Y-O>. The distortion of the Y polyhedron, $\langle \lambda_Y \rangle$, changes from 1.0169 to 1.0304 (with a mean value of 1.0244) and shows a negative correlation with $\Sigma^{Z}R^{2+}$ (Fig 10).

The <Y-O>$_{ideal}$ vs. <Y-O>$_{obs}$ diagram (Fig. 11) shows that the Y octahedron changes extensively from compressed through an unstrained to expanded state as a function of increasing Li content (Fig. 12).

Z site. In all samples, the <Z-O> mean bond distance shows a negative correlation with the ^{Z}Al content and a positive cor-

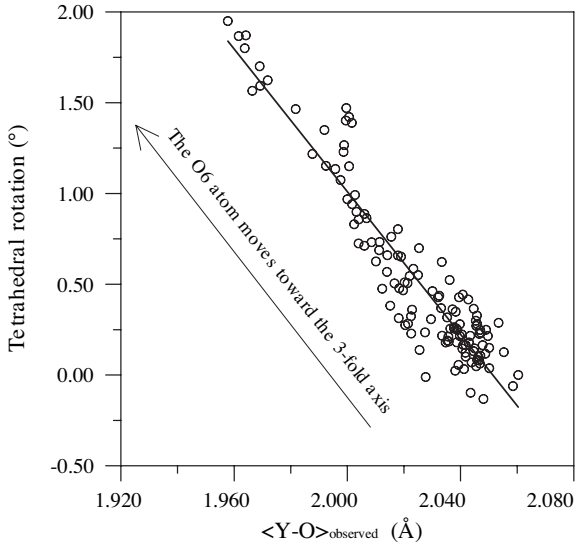

FIGURE 7. Because the Y cation is linked to the O6 atoms of two tetrahedra, any change in its size moves the O6 atom with respect to the threefold axis, producing a puckering of the ring. The tetrahedral angle rotation is measured from (0001) to normal to O4-O5 from O7 (Foit 1989).

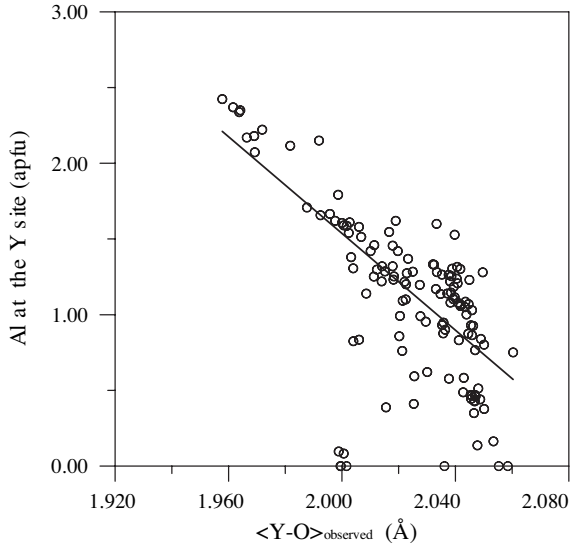

FIGURE 9. ^{Y}Al vs. $<Y\text{-}O>_{obs}$ plot showing the compositional dependence of the Y size. Line fitted to the data is only a guideline to the eye.

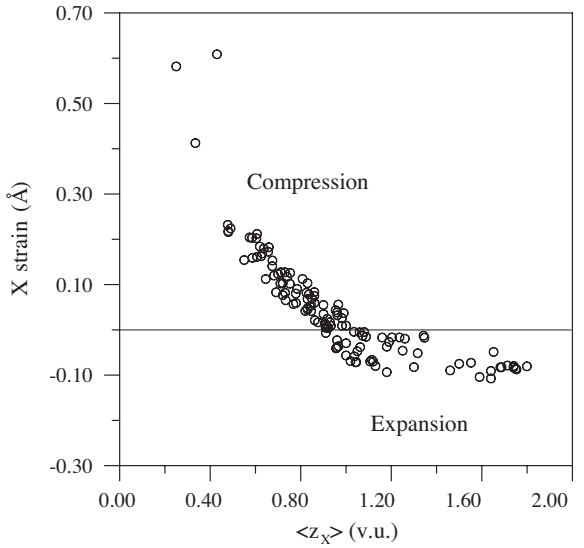

FIGURE 8. The relationship between X strain and $<z_X>$ shows that the expansion and compression of the X polyhedron change as a function of mean atomic valence at the X site. Solid horizontal line outlines unstrained state.

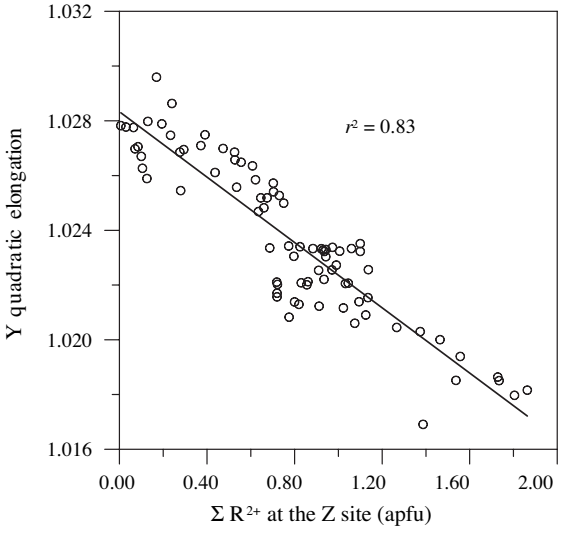

FIGURE 10. $<\lambda_Y>$ vs. $\Sigma^Z R^{2+}$ plot showing the influence of divalent cations in the Z site on Y quadratic elongation.

relation with $\Sigma^Z R^{2+}$(Fig. 13). The latter take on values up to 2.00 apfu, which seems to be the highest $\Sigma^Z R^{2+}$ content possible in tourmaline. This is also consistent with the end-members suggested by Hawthorne and Henry (1999). The lengths of the Z polyhedron edges show positive correlations with <Z-O>, except for those involving the O3 anion. In particular, the O3-O6 shared edge between Z and Y octahedra correlates much more strongly with <Y-O> than with <Z-O>. Distortion of the Z polyhedron may be expressed as quadratic elongation (Robinson et al. 1971) using the equation:

$$<\lambda_Z> = \sum_{i=1}^{6}\left[(\text{Z-O})_i / d_0\right]^2 \Big/ 6 \quad \text{or} \quad <\lambda_Z> = 1 + 2 \cdot \Delta d_Z / d_0$$

where $(\text{Z-O})_i$ are bond distances, Δd_Z is the increase in Z cation size due to distortion from a regular octahedron with a bond distance of $d_0 = (3/4\ V_Z)^{1/3}$, and a volume (V_Z), numerically equal to that of a real octahedron with bond distances $(\text{Z-O})_i$. In the samples studied, $<\lambda_Z>$ changes from 1.0112 to 1.0179, with a mean value of 1.0141, whereas the variation range of $\Delta d_Z \cong <\text{Z-O}> - d_0$ is 0.011–0.017 Å, with a mean value of 0.013 Å. In the samples

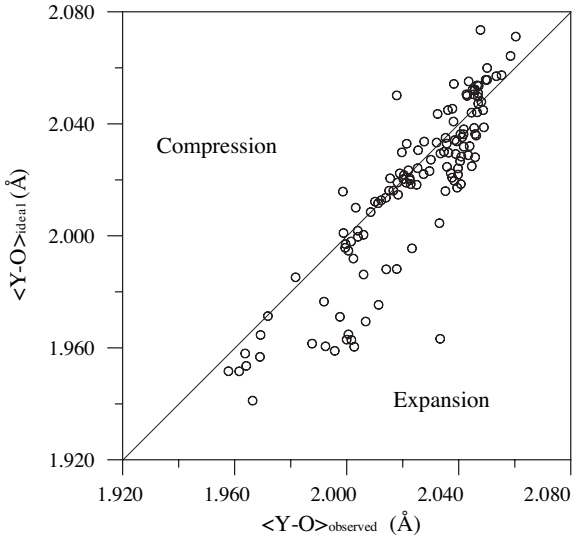

FIGURE 11. <Y-O>$_{ideal}$ vs. <Y-O>$_{obs}$ plot showing the strain state in the (YO_6) octahedra of tourmalines studied. Solid diagonal line: ratio 1:1 between <Y-O>$_{ideal}$ and <Y-O>$_{obs}$ outlining unstrained state.

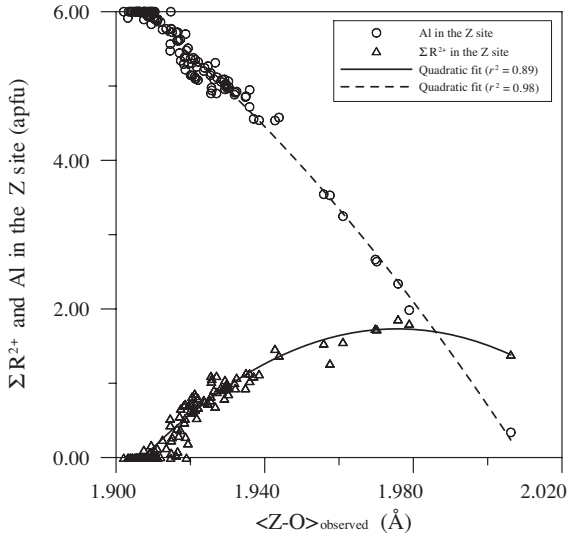

FIGURE 13. ^{Z}Al and $\Sigma^{Z}R^{2+}$ vs. <Z-O>$_{obs}$ plot showing the compositional dependence of the Z size.

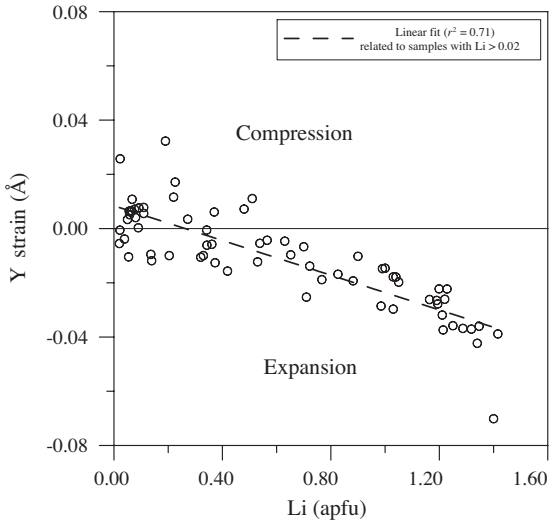

FIGURE 12. Relationships between Y strain (<Y-O>$_{ideal}$ – <Y-O>$_{obs}$) and Li content in tourmalines with Li > 0.02 apfu. Solid horizontal line outlines unstrained state.

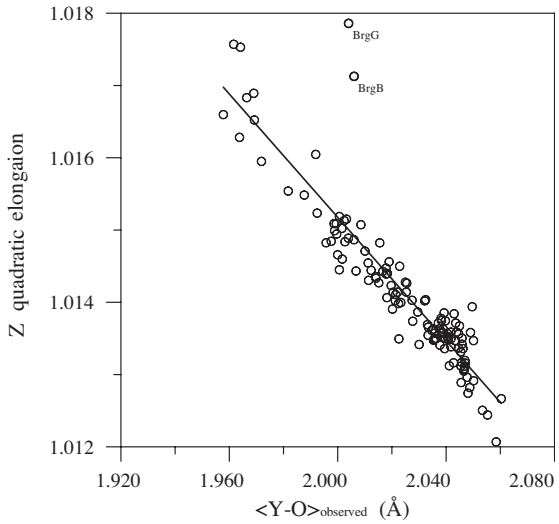

FIGURE 14. <λ_Z> vs. <Y-O>$_{obs}$ plot showing the variation of the Z distortion with the Y size.

with ^{Z}Al = 6 apfu, the mean value of d_0 is 1.893 Å. <Z-O> and its distortion is related by the following expression:

$$\frac{\text{Z-O}}{d_0} \underset{\cong}{+} \frac{\lambda_Z}{2} \quad \frac{1}{} \qquad (2)$$

Although <λ_Z> is strictly related to Z-O bond distances, it also shows an empirical relationship with <Y-O> (Fig. 14) in the samples studied (except for buergerite), according to the following equation:

$$<\lambda_Z> = 1.0975 - 0.0412 <\text{Y-O}> \ (r^2 = 0.92) \qquad (3)$$

Buergerite has a <λ_Z> value off the regression line because it has O^{2-} at the V site, whereas the other tourmalines have OH and different compositions in the first coordination sphere that influence quadratic elongation (Robinson et al. 1971). Combining and re-arranging the Equations 2 and 3, we can express the partial derivative of <Z-O> with respect to d_0 in the following way:

$$\frac{\partial <\text{Z-O}>}{\partial d_0} \cong 1.0488 - 0.0206 \cdot <\text{Y-O}>$$

This means that, for d_0 = constant, the variation of <Z-O> is inversely proportional to <Y-O>, consistent with the tendency of Y to compress Z.

The <Z-O>$_{ideal}$ vs. <Z-O>$_{obs}$ diagram (Fig. 15) shows that the Z octahedron is almost unstrained in samples with $\Sigma^{Z}R^{2+} < 0.40$

apfu (<Z-O>$_{obs}$ average deviation from the unstrained state is ca. 0.003 Å), whereas it is compressed in samples with $\Sigma^{Z}R^{2+}$ > 0.40 apfu (<Z-O>$_{obs}$ average deviation is ca. 0.009 Å). This result is consistent with the above inference concerning Al and Fe^{3+} ionic radii.

Crystal-chemical model for the Y and Z sites

Foit (1989) showed that the unit-cell volume of tourmaline varies as a function of the weighted-mean octahedral bond distances [(<Y-O> + 4 · <Z-O>)/5]. The present study confirms this statement. The structure comprises a framework of (ZO_6) octahedra, with channels parallel to the **c** axis. These channels are occupied by (YO_6) octahedra and other polyhedra (X, B, T), and the former show the greatest chemical variation. Consequently, the whole structure is stable if the channels of the Z framework are able to accommodate the Y cations.

Relation 1 suggests that one possible mechanism involves rotation of the tetrahedra that share O7 with the Z octahedra. As <Y-O> becomes larger, the less puckered the tetrahedral ring and the more the O7 atom is displaced away from Z, making the Z octahedron larger (Foit 1989). In fact, the Z-O7D bond distance (the largest among the Z-to-oxygen lengths) shows a negative correlation with ^{Y}Al (Fig. 16) and a positive correlation with <Y-O>. In samples with $\Sigma^{Z}R^{2+}$ < 0.40 apfu, Z-O7D and <Y-O> change according to the following equation:

$$Z\text{-}O7D = 1.2966 + 0.3232 \cdot \langle Y\text{-}O\rangle \quad (r^2 = 0.85) \qquad (4)$$

Consequently, if <Y-O> increases and <Z-O> does not change, the Z polyhedron will change its distortion in accordance with shifting of the O7 atom. In fact, Z-O7D shows a correlation with <λ_Z> (r^2= 0.83) in samples with $\Sigma^{Z}R^{2+}$ < 0.40 (i.e., ^{Z}Al ~ 6 apfu). However, the response of Z to the spatial requirement of Y is limited, because any increase in <Y-O> leads to a decrease in <λ_Z> (relation 3); this, in turn, leads to a smaller <Z-O> value (relation 2) in contrast to that suggested by relation 1. For this reason, the difference between <Y-O> and <Z-O> cannot be too large; otherwise <Z-O> will be too small to be commensurate with the shift of the O7 atom. In the samples studied, the difference between <Y-O> and <Z-O> varies from 0.023 to 0.142 Å. The latter value is the largest difference observed thus far in the tourmaline structure. It should be noted that <Y-O> is always larger than <Z-O>. On this basis, the two positively

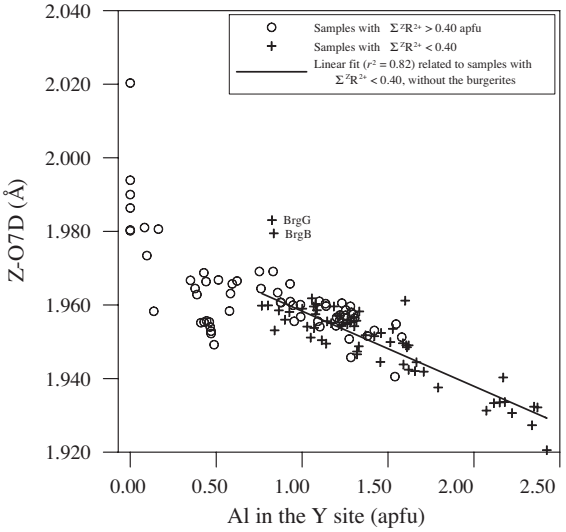

FIGURE 16. Z-O7D variations, given by the puckering of the tetrahedral ring (the tetrahedral rotation), reflect variations in ^{Y}Al content.

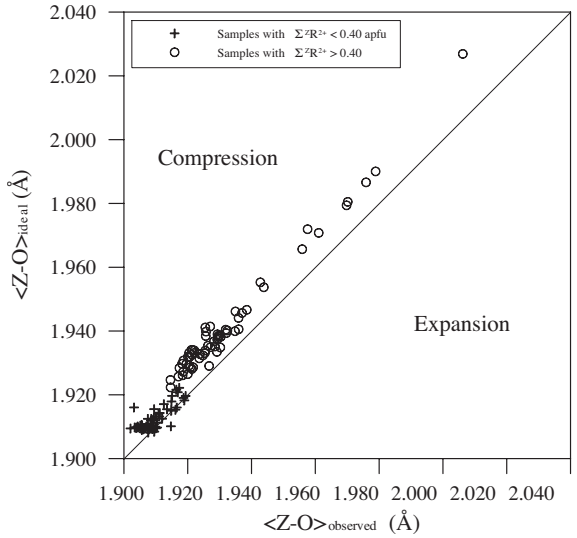

FIGURE 15. <Z-O>$_{ideal}$ vs. <Z-O>$_{obs}$ plot showing the strain state in the (ZO_6) octahedra of tourmalines studied. Solid diagonal line: ratio 1:1 between <Z-O>$_{ideal}$ and <Z-O>$_{obs}$ outlining unstrained state.

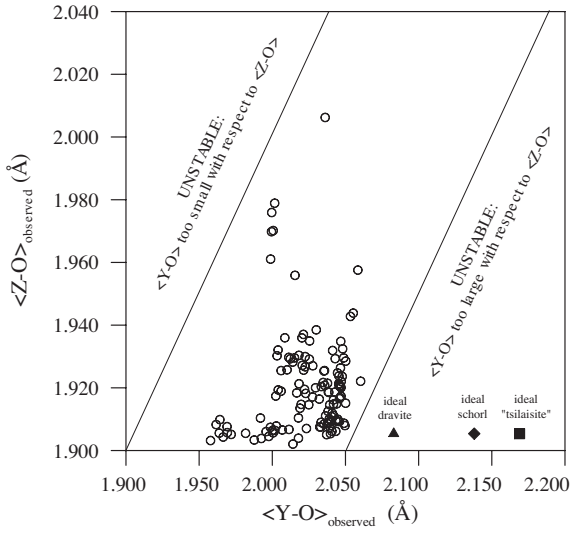

FIGURE 17. Relationship between <Z-O>$_{obs}$ and <Y-O>$_{obs}$, showing the structural-stability limits of the tourmaline group**.** The difference of 0.142 Å between <Y-O> and <Z-O> represents the maximum limit tolerated by the structure. Two solid diagonal lines: left = ratio 1:1 between <Z-O>$_{obs}$ and <Y-O>$_{obs}$; right = ratio shifted by 0.15 Å.

sloping lines in the <Z-O> vs. <Y-O> diagram (Fig. 17) mark the boundaries of the stability field of tourmaline. One possible mechanism to reduce the difference between <Y-O> and <Z-O> is the disordering reaction $^{Y}AL + {}^{Z}R \rightarrow {}^{Y}R + {}^{Z}AL$ (where R is R^{2+} or R^{3+}), which increases <Z-O> and decreases <Y-O>, because Al is the smallest cation present at the octahedral sites. As a consequence, the extent of solid solution also depends on the cation size mismatch at the Z site.

Instability of the end-members dravite, schorl, and "tsilaisite"

According to the present crystal-chemical model, the ideal end-members $Na^{Y}(Mg)_3{}^{Z}(Al)_6B_3Si_6O_{27}(OH)_4$ (dravite), $Na^{Y}(Fe^{2+})_3{}^{Z}(Al)_6B_3Si_6O_{27}(OH)_4$ (schorl), and $Na^{Y}(Mn^{2+})_3{}^{Z}(Al)_6B_3Si_6O_{27}(OH)_4$ ("tsilaisite"), are structurally unstable. Values of <Y-O> (2.083, 2.138, 2.169 Å) calculated from ionic radii for Mg, Fe^{2+}, and Mn^{2+} are too long, and incommensurate with <Z-O>. $\langle\lambda_Z\rangle$, calculated by relation 3, has the following values: 1.0117 (dravite), 1.0094 (schorl), and 1.0081 ("tsilaisite"). These distortions are small and lead to ^{Z}Al-O> values, calculated by relation 2, of 1.904 (dravite), 1.902 (schorl), and 1.901 Å ("tsilaisite"), which are incompatible with the above inference regarding ionic radii (e.g., Table 2) and the strain state of the Z bonds. Furthermore, relation 1 gives "anomalous" values of puckering (–0.62°, –1.70°, –2.31°, for dravite, schorl, "tsilaisite," respectively), indicating larger <Z-O> values. This result is consistent with relation 4, which leads to larger Z-O7D values (1.970, 1.988, 1.998 Å, for dravite, schorl, "tsilaisite," respectively) than those observed in samples with ^{Z}Al = 6 apfu (1.921 < Z-O7D < 1.961 Å). Last, the values of the O3-O6 edge, which change from 2.490 to 2.568 Å in tourmaline with ^{Z}Al = 6 apfu, do not fit those extrapolated using the regression equation, O3-O6 = 0.8126 <Y-O> + 0.9030 (r^2 = 0.94), obtained for 35 samples with ^{Z}Al = 6 apfu: 2.600 (dravite), 2.640 (schorl), and 2.667 Å ("tsilaisite"). In conclusion, all these geometrical results converge toward <Z-O> values larger than those consistent with Al. In other words, the channels of the $^{Z}(AlO_6)$ framework are too small to contain the $^{Y}(Mg)_3$, $^{Y}(Fe^{2+})_3$, and $^{Y}(Mn^{2+})_3$ configurations; consequently, <Y-O> and <Z-O> are incommensurate. This means that the bonds in Z cannot be adapted to the steric constraints given by large <Y-O>.

This is why, in nature, dravite always shows Mg and Al disordered over Y and Z sites, and schorl shows a maximum of 2–2.5 Fe^{2+} apfu, which is mostly ordered at the Y site and associated with an ^{Y}Al content of about 1 apfu in nearly all schorl samples. In addition, the "tsilasite" end-member seems more consistent with the $^{Y}(Mn^{2+}_{1.5}Al_{1.5})^{Z}(Al_6)$ composition (Schmetzer and Bank 1984) than the $^{Y}(Mn^{2+})_3{}^{Z}(Al_6)$. The former predicts a $Li \leftrightarrow Mn^{2+}$ substitution associated with the elbaite-tsilaisite series. This substitution is supported by the data of Bosi et al. (2005a), which show a slope of about 45 degrees in the $^{Y}Li \leftrightarrow {}^{Y}Mn^{2+}$ substitution in Mn-tourmalines. Furthermore, the <Y-O> value (2.04 Å), corresponding to the $^{Y}(Mn^{2+}_{1.5}Al_{1.5})$ composition, fits the above crystal-chemical model. The study of Choi and Grover (2006) on synthetic tourmaline supports the instability of tourmaline with a composition $^{Y}(Mn^{2+})_3{}^{Z}(Al_6)$. They report a Mn content of approximately 65 mol% end-member "tsilaisite," which is less than expected given the initial 100% bulk composition used in the synthesis.

Acknowledgments

The authors are indebted to Frank Hawthorne and Ulf Hålenius for the constructive suggestions on the manuscript. Associate Editor Darrell Henry, and the referees Franklin F. Foit and Andreas Ertl are thanked for constructive criticisms and comments. A special thanks goes to Massimiliano Arquilla, for his general support. This research was supported by a MURST grant, and carried out within the scientific programs of the Italian CNR, IGG-Rome.

References cited

Aurisicchio, C., Demartin, F., Ottolini, L., and Pezzotta, F. (1999) Homogeneous liddicoatite from Madagascar: a possible reference material? First EMPA, SIMS and SREF data. European Journal of Mineralogy, 11, 237–242.

Barton, R. Jr. (1969) Refinement of the crystal structure of buergerite and the absolute orientation of tourmalines. Acta Crystallographica, B25, 1524–1533.

Bloodaxe, E.S., Hughes, J.M., Dyar, M.D., Grew, E.S., and Guidotti, C.V. (1999) Linking structure and chemistry in the schorl-dravite series. American Mineralogist, 84, 922–928.

Bosi, F. and Lucchesi, S. (2004) Crystal chemistry of the schorl-dravite series. European Journal of Mineralogy, 16, 335–344.

Bosi, F., Lucchesi, S., and Reznitskii, L. (2004) Crystal chemistry of the dravite-chromdravite series. European Journal of Mineralogy, 16, 345–352.

Bosi, F., Agrosì, G., Lucchesi, S., Melchiorre G., and Scandale, E. (2005a) Mn-tourmaline from island of Elba (Italy). Crystal chemistry. American Mineralogist, 90, 1661–1668.

Bosi, F., Andreozzi, G.B., Federico, M., Graziani, G., and Lucchesi, S. (2005b) Crystal chemistry of the elbaite-schorl series. American Mineralogist, 90, 1784–1792.

Brese, N.E. and O'Keeffe, M. (1991) Bond-valence parameters for solids. Acta Crystallographica, B47, 192–197.

Brown, I.D. (2002) The chemical bond in inorganic chemistry: the bond valence model. International Union of Crystallography Monographs on Crystallography, 12, 288 p. Oxford University Press, U.K.

Brown, I.D. and Altermatt, D. (1985) Bond-valence parameters obtained from a systematic analysis of the Inorganic Crystal Structure Database. Acta Crystallographica, B41, 244–247.

Brown, I.D. and Shannon, R.D. (1973) Empirical bond-strength-bond-length curves for oxide. Acta Crystallographica, A29, 266–282.

Buerger, M.J., Burnham, C.W., and Peacor, D.R. (1962) Assessment of the several structures proposed for tourmaline. Acta Crystallographica, 15, 583–590.

Burns, P.C., MacDonald, D.J., and Hawthorne, F.C. (1994) The crystal-chemistry of manganese-bearing elbaite. Canadian Mineralogist, 32, 31–41.

Cámara, F., Ottolini, L., and Hawthorne, F.C. (2002) Crystal chemistry of three tourmalines by SREF, EMPA, and SIMS. American Mineralogist, 87, 1437–1442.

Cempírek, J., Novák, M., Ertl, A., Hughes, J.M., Rossman, G.R., and Dyar, M.D. (2006) Fe-bearing olenite with tetrahedrally coordinated Al from an abyssal pegmatite at Kutná Hora, Czech Republic: structure, crystal chemistry, optical and XANES spectra. Canadian Mineralogist, 44, 23–30.

Choi, J.B. and Grover, J. (2006) Synthesis and rietveld structure refinement of Mn-tourmalines (Tsilaisite). Journal of the Mineralogical Society of Korea, 19, 15–29.

Donnay, G. (1977) Structural mechanism of pyroelectricity in tourmaline. Acta Crystallographica, A, 33, 927–932.

Donnay, G. and Barton, R. Jr. (1972) Refinement of the crystal structure of elbaite and the mechanism of tourmaline solid solution. Tschermaks Mineralogische und Petrographische Mitteilungen, 18, 273–286.

Ertl, A. and Hughes, J.M. (2002) The crystal structure of an aluminum-rich schorl overgrown by boron-rich olenite from Koralpe, Styria, Austria. Mineralogy and Petrology, 75, 69–78.

Ertl, A., Hughes, J.M., Pertlik, F., Foit, F.F. Jr., Wright, S.E., Brandstätter, F., and Marler, B. (2002) Polyhedron distortions in tourmaline. Canadian Mineralogist, 40, 153–162.

Ertl, A., Hughes, J.M., Prowatke, S., Rossman, G.R., London, D., and Fritz, E.A. (2003a) Mn-rich tourmaline from Austria: structure, chemistry, optical spectra, and relations to synthetic solid solutions. American Mineralogist, 88, 1369–1376.

Ertl, A., Hughes, J.M., Brandstätter, F., Dyar, M.D., and Prasad, P.S.R. (2003b) Disordered Mg-bearing olenite from a granitic pegmatite from Goslarn, Austria: A chemical, structural, and infrared spectroscopic study. Canadian Mineralogist, 41, 1363–1370.

Ertl, A., Schuster, R., Prowatke, S., Brandstätter, F., Ludwig, T., Bernhardt, H.J., Koller, F., and Hughes, J.M. (2004a) Mn-rich tourmaline and fluorapatite in a Variscan pegmatite from Eibenstein an der Thaya, Bohemian massif, Lower Austria. European Journal of Mineralogy, 16, 551–560.

Ertl, A., Pertlik, F., Dyar, M.D., Prowatke, S., Hughes, J.M., Ludwig, T., and Bernhardt, H.-J. (2004b) Fe-rich olenite with tetrahedrally coordinated Fe^{3+} from Eibenstein, Austria: Structural, chemical, and Mössbauer data. Canadian Mineralogist, 42, 1057–1063.

Ertl, A., Rossman, G.R., Hughes, J.M, Prowatke, S., and Ludwig, T. (2005) Mn-bearing "oxy-rossmanite" with tetrahedrally coordinated Al and B from Austria: Structure, chemistry, and infrared and optical spectroscopic study. American Mineralogist, 90, 481–487.

Foit, F.F. Jr. (1989) Crystal chemistry of alkali-deficient schorl and tourmaline structural relationships. American Mineralogist, 74, 422–431.

Foit, F.F. and Rosenberg, P.F. (1979) The structure of vanadium-bearing tourmaline and its implications regarding tourmaline solid solutions. American Mineralogist, 64, 788–798.

Fortier, S. and Donnay, G. (1975) Schorl refinement showing composition dependence of the tourmaline structure. Canadian Mineralogist, 13, 173–177.

Francis, C.A., Dyar, M.D., Williams, M.L., and Hughes, J.M. (1999) The occurrence and crystal structure of foitite from a tungsten-bearing vein at Copper Mountain, Taos County, New Mexico. Canadian Mineralogist, 37, 1431–1438.

Gorskaya, M.G., Frank-Kamenetskaya, O.V., Rozhdestvenskaya, I.V., and Frank-Kamenetskii, V.A. (1982) Refinement of the crystal structure of Al-rich elbaite, and some aspects of the crystal chemistry of tourmalines. Soviet Physics—Crystallography, 27, 63–66.

Grice, J.D. and Ercit, T.S. (1993) Ordering of Fe and Mg in the tourmaline crystal structure: The correct formula. Neues Jahrbuch für Mineralogie Abhandlungen, 165, 245–266.

Grice, J.D. and Robinson, G.W. (1989) Feruvite, a new member of the tourmaline group, and its crystal structure. Canadian Mineralogist, 27, 199–203.

Grice, J.D., Ercit, T.S., and Hawthorne, F.C. (1993) Povondraite, a redefinition of the tourmaline ferridravite. American Mineralogist, 78, 433–436.

Hawthorne, F.C. and Henry, D. (1999) Classification of the minerals of the tourmaline group. European Journal of Mineralogy, 11, 201–215.

Hawthorne, F.C., MacDonald, D.J., and Burns, P.C. (1993) Reassignment of cation occupancies in tourmaline: Al-Mg disorder in the crystal structure of dravite. American Mineralogist, 78, 265–270.

Hill, R.J., Newton, M.D., and Gibbs, G.V. (1983) A crystal chemical study of stishovite. Journal of Solid State Chemistry, 47, 185–200.

Hughes, J.M., Ertl, A., Dyar, M.D., Grew, E.S., Shearer, C.K., Yates, M.G., and Guidotti, C.V. (2000) Tetrahedrally coordinated boron in a tourmaline: boron-rich olenite from Stoffhütte, Koralpe, Austria. Canadian Mineralogist, 38, 861–868.

Hughes, J.M., Ertl, A., Dyar, M.D., Grew, E.S., Wiedenbeck, M., and Brandstätter, F. (2004) Structural and chemical response to varying ^{4}B content in zoned Fe-bearing olenite from Koralpe, Austria. American Mineralogist, 49, 447–454.

Kahlenberg, V. and Veličkov, B. (2000) Structural investigations on a synthetic alkali-free hydrogen-deficient Fe-tourmaline (foitite). European Journal of Mineralogy, 12, 947–953.

London, D., Ertl, A., Hughes, J.M., Morgan VI, G.B., Fritz, E.A., and Harms, B.S. (2006) Synthetic Ag-rich tourmaline: Structure and chemistry. American Mineralogist, 91, 680–684.

MacDonald, D.J. and Hawthorne, F.C. (1995a) Cu-bearing tourmaline from Paraiba, Brazil. Acta Crystallographica, C51, 555–557.

——— (1995b) The crystal chemistry of Si ↔ Al substitution in tourmaline. Canadian Mineralogist, 33, 849–858.

MacDonald, D.J., Hawthorne, F.C., and Grice, J.D. (1993) Foitite, $\square(Al,Fe^{3+})Al_6Si_6O_{18}(BO_3)_3(OH)_4$, a new alkali-deficient tourmaline: Description and crystal structure. American Mineralogist, 78, 1299–1303.

Marler, B., Borowski, M., Wodara, U., and Schreyer, W. (2002) Synthetic tourmaline (olenite) with excess boron replacing silicon in the tetrahedral site: II. Structure analysis. European Journal of Mineralogy, 14, 763–771.

Marschall, H.R., Ertl A., Hughes, J.M., and McCammon, C. (2004) Metamorphic Na- and OH-rich disordered dravite with tetrahedral boron associated with omphacite, from Syros, Greece: chemistry and structure. European Journal of Mineralogy, 16, 817–823.

Nakatsuka, A., Yoshiasa, A., and Taken, S. (1995) Site preference of cations and structural variation in $Y_3Fe_{5-x}Ga_xO_{12}$ ($0 < x < 5$) solid solutions with garnet structure. Acta Crystallographica, B51, 737–745.

Nakatsuka, A., Yoshiasa, A., and Yamanaka, T. (1999) Cation distribution and crystal chemistry of $Y_3Al_{5-x}Ga_xO_{12}$ ($0 \le x \le 5$) garnet solid solutions. Acta Crystallographica, B55, 266–272.

Nuber, B. and Schmetzer, K. (1979) Die Gitterposition des Cr^{3+} im Turmalin: Strukturverfeinerung eines Cr-reichen Mg-Al-Turmalins. Neues Jahrbuch für Mineralogie Abhandlungen, 137, 184–197.

——— (1981) Strukturverfeinerung von Liddicoatit. Neues Jahrbuch fur Mineralogie Monatshefte, 215–219

——— (1984) Structural refinement of tsilaisite (manganese tourmaline). Neues Jahrbuch für Mineralogie Monatshefte, 301–304.

Robinson, K., Gibbs, G.V., and Ribbe, P.H. (1971) Quadratic elongation: a quantitative measure of distortion in coordination polyhedra. Science, 172, 567–570.

Schmetzer, K. and Bank, H. (1984) Crystal chemistry of tsilaisite (manganese tourmaline) from Zambia. Neues Jahrbuch für Mineralogie Monatshefte, 1984, 61–69.

Schmetzer, K., Nuber, B., and Abraham, K. (1979) Crystal chemistry of magnesium-rich tourmalines. Neues Jahrbuch für Mineralogie Abhandlungen, 136, 93–112.

Schreyer, W., Hughes, J.M., Bernhardt, H.-J., Kalt, A., Prowatke, S., and Ertl, A. (2002) Reexamination of olenite from the type locality: detection of boron in tetrahedral coordination. European Journal of Mineralogy, 14, 935–942.

Selway, J.B., Novàk, M., Hawthorne, F.C., Černý, P., Ottolini, L., and Kyser, T.K. (1998) Rossmanite, $(LiAl_2)Al_6(Si_6O_{18})(BO_3)_3(OH)_4$, a new alkali-deficient tourmaline: Description and crystal structure. American Mineralogist, 83, 896–900.

Shannon, R.D. (1976) Revised effective ionic radii and systematic studies of interatomic distances in halides and chalcogenides. Acta Crystallographica, A32, 751–767.

Taylor, M.C., Cooper, M.A., and Hawthorne, F.C. (1995) Local charge-compensation in hydroxy-deficient uvite. Canadian Mineralogist, 33, 1215–1221.

Tippe, A. and Hamilton, W.C. (1971) A neutron diffraction study of the ferric tourmaline, buergerite. American Mineralogist, 56, 101–113.

Tossel, J.A. and Gibbs, G.V. (1977) Molecular orbital studies of geometries and spectra of minerals and inorganic compounds. Physics and Chemistry of Minerals, 2, 21–57.

Wright, S.E., Foley, J.A., and Hughes, J.M. (2000) Optimization of site occupancies in minerals using quadratic programming. American Mineralogist, 85, 524–531.

Manuscript received June 28, 2006
Manuscript accepted January 31, 2007
Manuscript handled by Darrell Henry